Advances in Science and Technology Research Journal

Advances in Science and Technology Research Journal, 2027, 21(1), 212–224
https://doi.org/10.12913/22998624/231502
ISSN 2299-8624, License CC-BY 4.0

Received: 2026.07.31
Accepted: 2026.11.15
Published: 2026.12.01

Influence of bore-to-stroke ratio and crank mechanism design on the performance of an alpha-type Stirling cryocooler

Jacek Kropiwnicki[1*], Michał Śmieja[2]

[1] Institute of Energy, Faculty of Mechanical Engineering and Ship Technology, Gdańsk University of Technology, ul. Gabriela Narutowicza 11/12, Gdańsk, 80-233, Poland
[2] Department of Mechatronics, Faculty of Technical Sciences, University of Warmia and Mazury, ul. Michała Oczapowskiego 11, 10-719 Olsztyn, Poland
* Corresponding author's e-mail: jkropiwn@pg.edu.pl

ABSTRACT

The performance of alpha-type Stirling cryocoolers is strongly influenced by both thermodynamic and mechanical design parameters. This paper investigated the effect of the bore-to-stroke ratio on the cooling output of a cryogenic Stirling device while maintaining a constant swept volume of the compression space. An isothermal thermodynamic model was employed to evaluate pressure variations and cooling output for different piston diameters and head clearances. The results show that increasing the bore-to-stroke ratio reduces cooling output because of the associated increase in dead volume. However, for head clearances below 0.15 mm, this effect becomes significantly less pronounced, enabling larger piston diameters and shorter strokes to reduce the overall dimensions and mass of the device. The influence of the bore-to-stroke ratio on piston side loading was also analysed by evaluating the normal force acting on the piston guiding section. Although larger bore-to-stroke ratios improve the durability of the piston-cylinder pair by reducing surface pressure, they simultaneously decrease cooling performance, indicating the existence of an optimal design compromise. Furthermore, crankshaft axis eccentricity and a balance-shaft system were investigated as methods for reducing piston side forces. A crankshaft axis eccentricity of −0.2 mm combined with second-order balance shafts reduced the normal-force amplitude by up to 63% compared with the conventional mechanism. The results indicate that an appropriate combination of geometric and crank-mechanism parameters can provide a favourable compromise between thermodynamic performance, piston side loading, and vibration-related forces.

Keywords: Stirling devices, cryocoolers, cooling output.

INTRODUCTION

The optimisation and technological development of Stirling cycle devices represent a vital frontier in modern cryogenic engineering and thermal science, driven by expanding applications across defence sectors, aerospace missions, and large-scale industrial infrastructure [1, 2]. These systems operate on a closed regenerative thermodynamic cycle that leverages the periodic compression and expansion of a working fluid, typically helium, to achieve efficient refrigeration or generate mechanical power. Figure 1 shows the reversed Stirling thermodynamic cycle used in cryocoolers. The structural architecture and operational parameters of these devices fundamentally govern their thermodynamic behaviour, significantly influencing key performance metrics such as the coefficient of performance, relative Carnot efficiency, and net cooling capacity. Achieving high operational efficiency requires an explicit understanding of how individual geometric and operational parameters interact dynamically with a multitude of intrinsic mechanical and thermal losses. A central focus in miniature Stirling cryocooler research is the refinement of configurations conforming to strict size, weight, and power limitations, which are essential for contemporary high-operating temperature infrared detector systems and standard military or

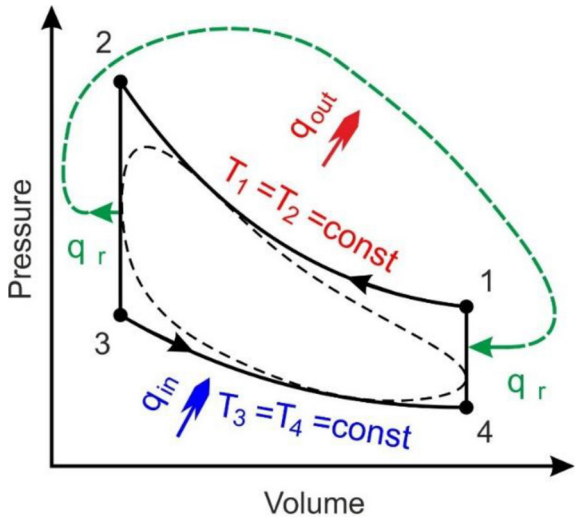


Figure 1. Reversed Stirling thermodynamic cycle

scientific imaging arrays [3]. Parametric studies utilising semi-adiabatic thermodynamic models reveal that fluid flow pressure loss typically constitutes the largest power loss within miniature rotary units, whereas regenerator axial conduction represents the primary source of thermal degradation. Every variation in piston stroke length and regenerator length manifests as a substantial shift in both overall performance and device compactness [4]. As the operating speed of a rotary Stirling device increases, the cooling capacity scales in a nearly linear fashion; however, this capacity expansion is accompanied by an exponential surge in fluid pressure drops and mechanical friction losses, which eventually suppresses the coefficient of performance and sets a distinct upper bound for efficient operation. Meticulous geometric optimisation of these parameters can yield highly efficient, compact systems, such as a miniature cryocooler weighing a mere 177 grams capable of generating 0.68 W of net refrigeration at a cooling temperature of 150 K, requiring an actual input power of 4.28 W, which yields a predicted coefficient of performance of 15.85% [4].

The efficiency of the entire thermodynamic cycle is heavily dependent on the trade-off between heat transfer maximisation and aerodynamic pressure drop reduction in the regenerator [5, 6]. Design strategies over recent years have shifted toward investigating uniform and non-uniform mesh matrices, porous morphology optimisation, and the mitigating effects of non-ideal structural parameters on the overall system performance under stringent size, weight, and power (SWaP) constraints [7, 8]. Experimental and parametric assessments indicate that uniform mesh regenerators require meticulous number optimisation [9]. Longitudinal conduction losses along the metal screen stack can increase the intrinsic in-efficiency of the regenerator component by up to 137 percent [8]. Standard models assuming constant material constants underestimate matrix temperature swings and localised in-efficiencies by significant margins; fully resolved cyclic simulations indicate that temperature swings can be up to 185 percent higher when accounting for realistic temperature-dependent properties [8]. The physical characteristics of the regenerator, including the selection of stainless steel wire mesh parameters, such as a mesh size number of 400 (per inch), a wire diameter matched to high volumetric thermal efficiency, and an internal tube diameter of 6.5 mm, directly manage the balance between effective heat storage and fluid resistance [10]. To accurately predict these transient phenomena, advanced theoretical models of rotary-integral Stirling cryocoolers evaluate the dynamic variation of thermodynamic properties [11]. Refining the calculation of porosity and volumetric heat transfer area for wire mesh regenerators enables a more precise assessment of cooling capacity and temperature limits. Treating the thermophysical properties of both the working gas and the surrounding metal matrix as temperature and pressure-dependent functions shows that increases in stroke length and mesh density significantly enhance capacity, while an optimised geometric envelope allows the system to achieve its intended temperature targets while maintaining structural integrity during rapid cyclic oscillations [11].

Expanding upon these foundational relations, comprehensive energy and exergy balance models incorporating a unified time-step evaluation show that mechanical friction stands as the most severe mechanical loss, while parasitic conduction through the displacer wall and regenerator column represents the most critical thermal leak [12]. The operational envelope is shaped by several variables, including the temperature differential between the cold end and hot end, the mean system pressure, the rotational frequency, the displacer clearance gap, and the phase shift between the compression piston and the expansion displacer. Additionally, the geometric ratio between the piston diameter and its stroke length serves as a primary lever for tuning the swept volume. Modulating these features helps suppress severe

operational losses, such as gas spring hysteresis, displacer shuttle heat transport, and clearance seal heat pumping, all of which dynamically interact to degrade the net coefficient of performance if the components are misaligned [12]. When scaling these devices for high-capacity industrial systems, such as capturing boil-off methane gas from liquefied natural gas storage units, the design priorities shift toward maximising absolute cooling power and maximising relative Carnot efficiency. Large-scale single-stage Stirling cryocoolers are capable of delivering up to 1050 W of cooling capacity at 77 K while achieving a relative Carnot efficiency of 33.28% [13]. The scalability and efficiency of free-piston Stirling coolers operating at intermediate cryogenic ranges have also seen major advancements through careful parametric design of the core heat exchangers and regenerators. A high-efficiency free-piston Stirling cooler based on thermoacoustic principles can achieve a massive cooling capacity of 350 W at 80 K while operating with an input electric power of 3.57 kW, demonstrating a relative Carnot efficiency of 26.8% that underscores the feasibility of using high-capacity Stirling systems for cooling high-temperature superconductors [14]. The performance of such large-scale coolers is heavily dictated by internal geometry, where parametric analysis focuses on the wire mesh number, the porosity of the regenerator matrix, and the displacer clearance gap. Increasing the wire mesh number enhances the heat transfer area but simultaneously amplifies the fluid flow pressure drop, meaning that an optimal balance must be struck to maximise the net refrigeration output [15]. Furthermore, the displacer clearance gap must be tightly controlled because excessive clearance leads to parasitic gas leakage and enthalpy loss, whereas an overly tight clearance increases mechanical friction and manufacturing complexity [15]. These findings are supported by quantitative evaluations based on dimensionless analysis methods alongside experimental validation to evaluate entropy generation within a free-piston Stirling cooler. This entropy generation analysis confirms that the regenerator and the associated heat exchangers are the primary sites of irreversibility, and that optimising the characteristic scales of the system can systematically minimise thermal and viscous losses, thereby driving up the overall coefficient of performance [16].

A critical design innovation in ultra-low temperature Stirling-type pulse tube coolers is the implementation of multi-stage thermal coupling combined with advanced phase-shifting configurations to enhance performance at extremely low temperatures. A twenty Kelvin high-capacity thermally-coupled Stirling-type pulse tube cooler designed specifically for applications such as superconductivity and zero-boil-off liquid hydrogen storage systems can utilise ambient displacers to maximize the thermodynamic performance of the low-temperature stage by pre-cooling both its regenerator and pulse tube. System performance under this configuration is highly sensitive to the average charging pressure, operating frequency, and the precise pre-cooling temperature achieved by the first stage. An experimental prototype of this nature demonstrated a minimum no-load temperature of 11.5 K and achieved a substantial cooling power of 8.4 W at 20 K when supplied with an input electrical power of 2256 W [17]. At higher refrigeration temperatures, such as those required for ultra-low temperature cold storage, alternative phase-shifting mechanisms can be used to drastically enhance efficiency and cooling capacity. A high-capacity Stirling-type pulse tube refrigerator operating at 173 K can incorporate a passive rod displacer that serves as a highly efficient substitute for traditional inertance tubes, offering the capability for acoustic power recovery within the system. An optimised design of this type yielded an impressive cooling capacity of 157.5 W at 173 K with an input electric power of only 500 W, representing a remarkable relative Carnot efficiency of 21.8% [18].

The continuous operation of high-power free-piston Stirling machines requires robust thermal management of their internal electrical components, particularly the linear alternator, because excessive temperature rises can degrade permanent magnets and compromise the overall system stability. Numerical and experimental studies focusing on the cooling enhancement of a high-power linear alternator reveal severe non-uniformity in the internal gas flow, which induces localised hot spots near the electrical coils and permanent magnets [19]. The implementation of these optimised geometric features increased the convective heat transfer coefficients of the coil and magnet walls by over 10%, which subsequently reduced the maximum operating temperatures of the coils by 32.5 K and the magnets by 13.2 K [19]. Under high-pressure conditions up to 4.5 MPa, the oscillating helium flow interacts complexly with the solid boundaries, making

traditional convective cooling insufficient [20]. The introduction of the high-emissivity coating successfully altered the internal energy balance, reducing the maximum internal temperature of the coil from 395 K down to 385 K, while the magnet temperature decreased from 363 K to 353.8 K [20].

Innovations in Stirling technology also extend to hybrid architectures that pair Stirling drive units with alternative cryogenic configurations to exploit the distinct advantages of different thermodynamic cycles [4, 21]. For example, a Stirling/pulse tube hybrid cryocooler merges the high-efficiency character of a Stirling driver with the high-reliability, moving-part-free nature of a pulse tube cold finger, an arrangement highly attractive for space missions that enforce strict structural and power envelopes [22]. Further integration of Stirling principles is observed in thermoacoustic heat-driven systems, such as a resonance tube-coupled free-piston Stirling engine-based combined cooling and power unit [23]. This approach replaces traditional rigid mechanical linkages with a resonance tube that couples a free-piston Stirling engine to a cryogenic cooler, introducing a linear alternator to facilitate system startup and manage varied auxiliary loads. When operated at a mean helium pressure of 5 MPa and an engine heating temperature of 833 K, such a resonance-coupled configuration can provide a cooling capacity of 1000 W at 110 K while simultaneously generating 800 W of electric power, demonstrating an overall global exergy efficiency of 29.4% through precise acoustic power matching among the subsystems [23].

In addition to single-axis machines, upscaling can be achieved through the coupling of multiple thermoacoustic and Stirling units, such as the upscaling of thermoacoustic-Stirling duplex cryocoolers based on resonance tube coupling. A duplex system eliminates moving mechanical parts in the driver stage by using a thermoacoustic heat engine to directly power a Stirling cryocooler via acoustic work. An active displacer method can be proposed for optimising the acoustic impedance matching between the engine and the cooler stages. A prototype featuring a compact coiled resonance tube demonstrated that proper tuning of the resonance tube length and diameter allows the system to deliver high cooling capacities, achieving a remarkable cooling power of 380 W at 80 K, outperforming previous configurations and providing a highly reliable, oil-free solution for large-scale cryogenic cooling [24]. Understanding and controlling these thermoconvective effects is crucial for ensuring the reliable self-nucleation of oscillations, which directly influences the transient response and operational window of the coupled Stirling refrigeration system [25]. In these multi-stage configurations, a double-stage Stirling cooler is utilised to provide a stable thermal sink at approximately 20 K, which allows subsequent Joule-Thomson loops utilising straight, long counter-flow heat exchangers to efficiently reach 4.5 K or 1.7 K [26]. Ultimately, micro-cryogenic cooling research indicates that while micro-Joule-Thomson systems driven by high-frequency micro-compressors offer excellent spatial scaling, miniature Stirling devices maintain an exceptional baseline for raw efficiency and thermodynamic robustness [3]. The ongoing refinement of Stirling design features, specifically the optimisation of the regenerator matrix to manage the fine balance between flow friction and thermal storage, remains the primary pathway for improving the coefficient of performance and extending the cooling capacity across all scales of cryogenic deployment, because each architectural decision directly dictates the balance between power recovery and parasitic losses. Minimising irreversibilities due to pressure drops, thermal conduction, and flow maldistribution remains the primary vector for maximising the coefficient of performance and unlocking the full potential of Stirling cooling technology across all scales and operating temperatures.

In this work, particular attention is paid to the influence of such geometrical features of the Stirling microcooler as the bore-to-stroke ratio and clearance between the piston and the cylinder head on the cooling output of the device. Furthermore, it was noted that in the case of alpha-type Stirling devices, comprehensive information on possible methods for reducing vibrations due to the presence of an unbalanced normal force in the crank mechanism, occurring between the connecting rod and the piston, is lacking. This paper presented an analysis of the use of several design methods for reducing this force. While prior studies focused on general operational variables such as charging pressure, rotational frequency, or regenerator dimensions, this research specifically evaluated surface pressure on the piston guiding section to balance thermodynamic cooling output against piston-cylinder mechanical load.

ISOTHERMAL ANALYSIS

For analytical modelling of Stirling devices, isothermal and adiabatic models are most often used [27, 28]. Apart from the regenerator, which is crucial to the device's operation, there are no separate heat exchangers outside the compression and expansion spaces. The cylinders and heads of these spaces constitute the basic heat exchange surfaces. Furthermore, the temperature in the compression and expansion cylinders is subject to very little change. For this reason, the isothermal model is considered more useful for preliminary analysis for alpha-type cryocooler applications [1]. The isothermal model used in this study is appropriate for preliminary parametric analysis because it allows the influence of bore-to-stroke ratio and head clearance on the thermodynamic cycle to be evaluated with relatively low computational complexity. However, it assumes constant gas temperatures in the compression and expansion spaces and therefore does not account explicitly for finite rate heat transfer, cycle temperature variations, etc. Consequently, the calculated cooling output should primarily be regarded as a comparative measure rather than an exact prediction of the performance of a real cryocooler. An adiabatic or more advanced model [29] incorporating transient heat transfer, regenerator losses, pressure drops, and other parasitic effects could change both the predicted cooling output and the quantitative dependence on bore-to-stroke ratio. Therefore, the optimum value obtained in this study should be considered applicable to the assumptions of the present preliminary model and should be verified using a higher-fidelity thermodynamic model before final design.

In isothermal analysis, it is assumed that the temperature in the separated working spaces is constant, and the mass of the working medium is assumed to be constant [1]:

$$m_t = m_e + m_d + m_c \tag{1}$$

where: m_t – total mass of the working gas, m_e – mass of the working gas in the expansion space, m_d – mass of the working gas in the dead space (including regenerator), m_c – mass of the working gas in the compression space.

Assuming that the pressure in all spaces is the same, the instantaneous pressure can be determined from the previous equation:

$$p = m_t \cdot R_g \cdot \left(\frac{V_e}{T_E} + \frac{V_D}{T_D} + \frac{V_c}{T_C}\right)^{-1} \tag{2}$$

where: R_g – individual gas constant of the working gas, V_e – volume of the expansion space:

$$V_e = \frac{1}{2} \cdot V_E \cdot \left(1 + cos(\varphi)\right) \tag{3}$$

where: V_E – swept volume in the expansion space, φ – crank angle, V_D – volume of regenerator, and associated ducts and ports, V_C – volume of the compression space:

$$V_c = \frac{1}{2} \cdot V_C \cdot \left(1 + cos(\varphi - \propto)\right) \tag{4}$$

where: V_C – swept volume in the compression space, α – angle by which volume variations in the expansion space lead to those in the compression space, T_E, T_C – temperature of the working gas in the specified space: expansion, compression, T_D – temperature of the working gas in the dead space.

It is assumed that temperature variation in the dead space is linear in the axial direction, then the mean temperature can be given by:

$$T_D = T_C + \frac{1}{2} \cdot (T_E - T_C) \tag{5}$$

The calculations can be made easier by defining the following:

Swept volume ratio:

$$k = \frac{V_C}{V_E} \tag{6}$$

Temperature ratio:

$$\tau = \frac{T_C}{T_E} \tag{7}$$

Dead volume ratio:

$$X = \frac{V_D}{V_E} \tag{8}$$

Reduced dead volume:

$$S_D = \frac{V_D}{V_E} \tag{9}$$

$$\delta = \frac{\sqrt{\tau^2 + k^2 + 2 \cdot \tau \cdot k + 2 \cdot S_D}}{\tau + k + 2 \cdot S_D} \tag{10}$$

$$\theta = tan^{-1}\left(\frac{k \cdot \sin(\alpha)}{\tau + k \cdot \cos(\alpha)}\right) \tag{11}$$

$$p_{max} = p_{mean}\sqrt{\frac{1+\delta}{1-\delta}} \quad (12)$$

where: p_{mean} – mean cycle pressure.

Cooling output of the device was determined using the following equation:

$$Q_e = \frac{V_E \cdot p_{mean} \cdot \delta \cdot \pi \cdot \sin(\theta)}{\sqrt{(1-\delta^2)}+1} \quad (13)$$

Instantaneous pressure can be calculated as a function of the crank angle:

$$p = p_{max}\frac{1-\delta}{1+\delta \cdot \cos(\varphi-\theta)} \quad (14)$$

IMPACT OF THE BORE-TO-STROKE RATIO ON THE COOLING OUTPUT OF THE CRYOGENIC STIRLING DEVICE

The paper analysed the design of the alpha-type Stirling device, which in commercial solutions is most often called a rotary Stirling cryocooler. Figure 2 shows the device under consideration, with the heat supply and removal areas marked, as well as the basic design dimensions used in the analysis. The analysis assumed the design parameters of the device presented in Table 1.

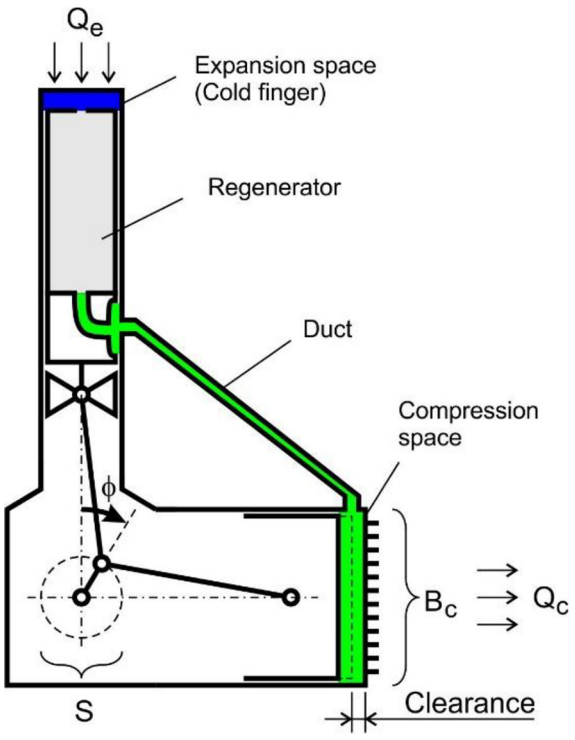


Figure 2. Stirling cryocooler type alpha: B_c/S – bore/stroke of the compression piston; Q_e – heat delivered (cooling output); Q_c – heat removed

The impact of bore-to-stroke ratio on the cooling output of a cryogenic Stirling device will be analysed below. By increasing the diameter of the compression space piston, its stroke can be reduced, while maintaining the same swept volume. This consequently allows for a reduction in the dimensions and weight of the entire device [10].

Based on an isothermal Stirling engine model presented in the previous section, pressure changes in the working space were determined. The analysis assumed that the swept volume of the compression and expansion spaces would be constant. By changing the bore of the compression space, the piston stroke would be modified so that the swept volume of the compression space remained constant. Changing the piston diameter results in a change in the dead volume above the piston, which automatically changes the total dead volume and affects the cooling output of the device. One of the key parameters affecting dead space is the clearance between the piston and the cylinder head. This work assumes that the clearance in the compression and expansion spaces is the same, but due to the large disproportion between the swept volume of the compression space and the expansion space, it can be assumed that the clearance in the compression space has a decisive influence on dead space. Figure 3 shows the p-V diagram for one of the analysed cases.

Based on the calculated pressure-volume curve, the cooling output (Q_e) of the device was determined using an isothermal model.

The analysis considered 7 bore-to-stroke ratio values, starting with a piston diameter of 10 mm, which changed by 2 mm at each point, until it reached a final value of 22 mm. Assuming a constant swept volume, the piston stroke was calculated for each assumed piston diameter, followed

Table 1. Design parameters of the Stirling cryocooler

Parameter	Value
Ambient temperature	303 K
Cold-tip temperature	73 K
Charge pressure	2.5 MPa
Phase angle	90 deg
Nominal speed	3000 rpm
Swept volume – compression space	402 mm^3
Swept volume – expansion space	101 mm^3
Regenerator volume	276 mm^3
Duct volume	79 mm^3
Connecting rod length	20 mm

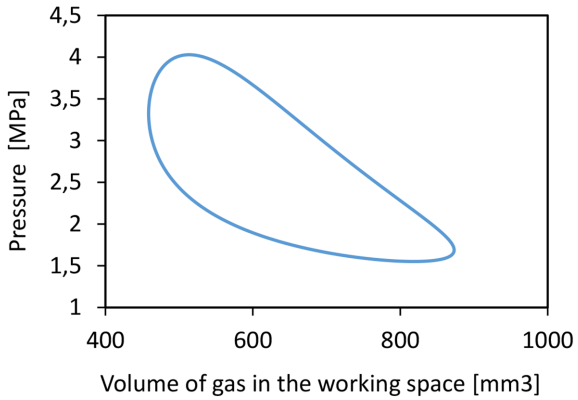


Figure 3. P-V diagram; bore-to-stroke ratio 8.0, clearance 0.25 mm

by the bore-to-stroke ratio. A summary of the analysed cases is provided in Table 2.

Figure 4 presents the calculation results, with the piston diameter in the compression chamber modified within a range of 10–22 mm, while maintaining a constant swept volume. Furthermore, the clearance between the piston and the cylinder head was also modified.

Based on the obtained results, it can be concluded that for typical clearance values applied in microcryocoolers, cooling output decreases significantly with increasing bore-to-stroke ratio. For significantly reduced clearances, below 0.15 mm, this influence is less noticeable, meaning that a larger piston and shorter stroke can be used, reducing device mass and dimensions. Changing the bore-to-stroke ratio also changes the surface pressure on the piston guiding section, which is one of the main factors influencing the friction forces between the piston and the cylinder liner, and consequently, the system's durability. Figure 5 shows the distribution of forces in the crank mechanism of the compression chamber, resulting from the effect of the pressure difference between the compression chamber and the buffer chamber (under the piston) on the piston crown. Inertial forces of the reciprocating masses were also taken into consideration. The normal force (N) acting on the piston pin can be defined as follows:

Table 2. Summary of the analysed cases

Diameter [mm]	Stroke [mm]	Bore-to-stroke ratio [-]
10	5.12	1.95
12	3.56	3.38
14	2.61	5.36
16	2.00	8.00
18	1.58	11.39
20	1.28	15.62
22	1.06	20.80

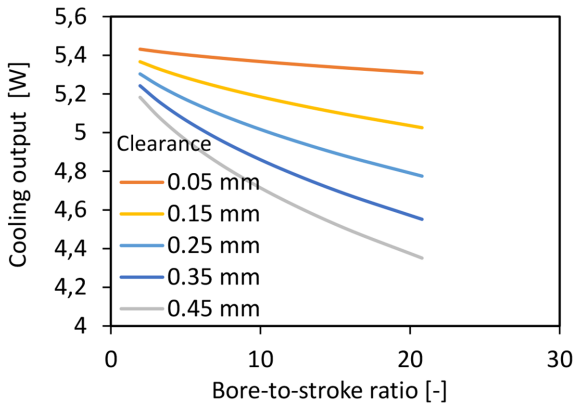


Figure 4. Influence of bore-to-stroke ratio on cooling output (Q_e); constant swept volume

$$N(\varphi) = \left\{\left[(p(\varphi) - p_o) \cdot S_p\right] + \left[P_{in}(\varphi)\right]\right\} \cdot \cdot \tan\left\{asin\left[\frac{R}{L_r} \cdot sin(\varphi - \alpha)\right]\right\} \quad (15)$$

where: p – gas pressure over the piston, p_o – gas pressure in the buffer space (under the piston), S_p – piston surface, P_{in} – inertial forces of the reciprocating masses, α – angular shift between the movement of working elements in the expansion and compression spaces, assumed to be 90 deg, φ – angle between the cylinder axis and the crank arm for the expansion cylinder.

This normal force can then be used to calculate the surface pressure on the piston guiding section:

$$\sigma_p(\varphi) = \frac{N(\varphi)}{L_p \cdot B_c} \quad (16)$$

where: B_C – bore of the compression space, L_p – length of the piston guiding section.

It was assumed that the ratio of the length of the piston guiding section to the bore of the compression space is constant:

$$\frac{L_p}{B_c} = 0.75 \quad (17)$$

Figure 6 shows the course of the surface pressure on the piston guiding section caused by variable working gas pressure and inertial forces for a bore-to-stroke ratio of 8.0, clearance of 0.25 mm.

Figure 7 presents the results of an analysis of the effect of the bore-to-stroke ratio on the surface

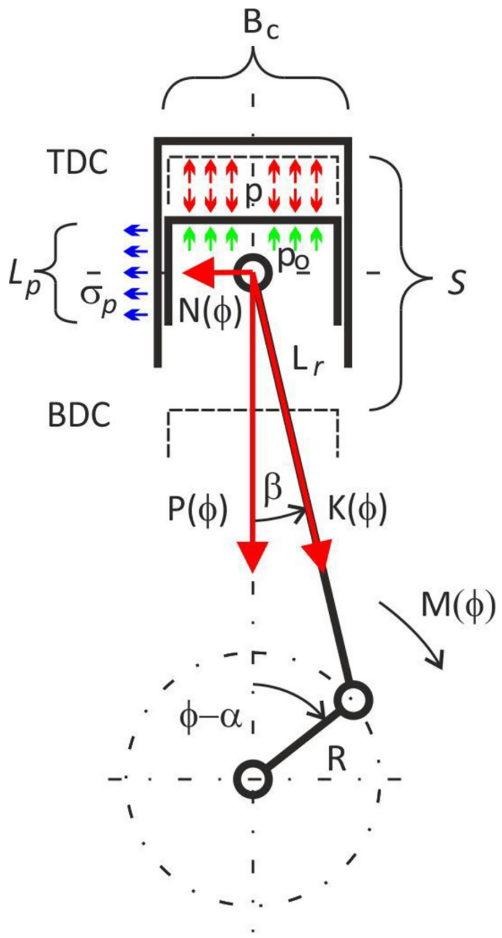


Figure 5. Compression space crank mechanism along with the forces acting on the system

pressure on the piston guiding section. Due to the strong relationship between the surface pressure on the piston guiding section and the durability of the piston-cylinder friction pair, the results are presented using the inverse of this quantity. Figure 7 also presents the influence of the bore-to-stroke ratio on cooling output for a fixed clearance of 0.25 mm. Based on the obtained results, it can be concluded that for lower, technically achievable clearance values, the bore-to-stroke ratio negatively impacts cooling output, but at the same time increases the inverse surface pressure on the piston guiding section, which increases the device's durability.

Cooling output represents the primary thermodynamic function of the cryocooler, whereas reduced piston side loading improves the durability and friction characteristics of the piston-cylinder pair. Since these objectives vary in opposite directions with increasing bore-to-stroke ratio, equal weighting provides a balanced compromise for preliminary design when no application-specific priority has been established. However, the appropriate weighting is application-dependent. For systems in which maximum refrigeration capacity is the dominant requirement, greater weight should be assigned to cooling output, whereas applications emphasising long service life, reliability, or reduced friction may justify greater weight for mechanical loading. For example, in spacecraft and defence electronics, maximum service life and reliability will be prioritised over thermodynamic efficiency. Assuming equal weights for both analysed parameters, it can be concluded that a bore-to-stroke ratio of 15 is the optimal value for the considered clearance of 0.25 mm.

INFLUENCE OF THE CRANK MECHANISM DESIGN ON THE PERFORMANCE OF A STIRLING CRYOCOOLER

In the following section, shifting the crankshaft axis relative to the cylinder axis of the compression space was considered to reduce the normal force on

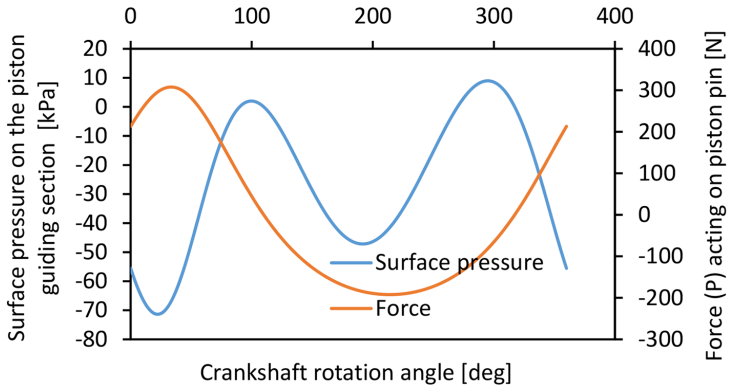


Figure 6. Surface pressure on the piston guiding section, and force acting on piston pin caused by variable working gas pressure and inertial forces for a bore-to-stroke ratio of 8.0, clearance of 0.25 mm

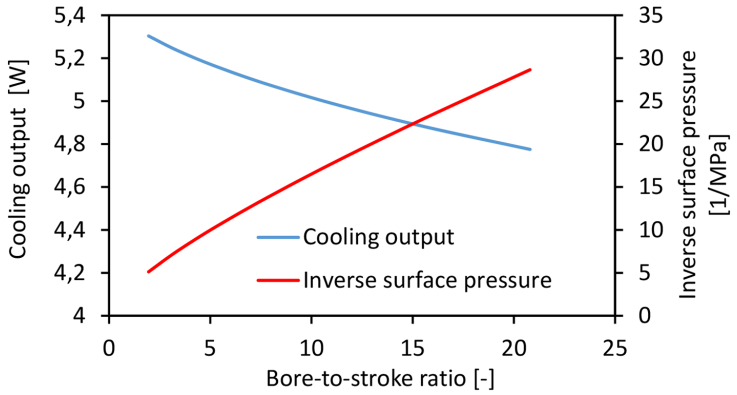


Figure 7. Influence of bore-to-stroke ratio on inverse surface pressure and cooling output, clearance 0.25 mm

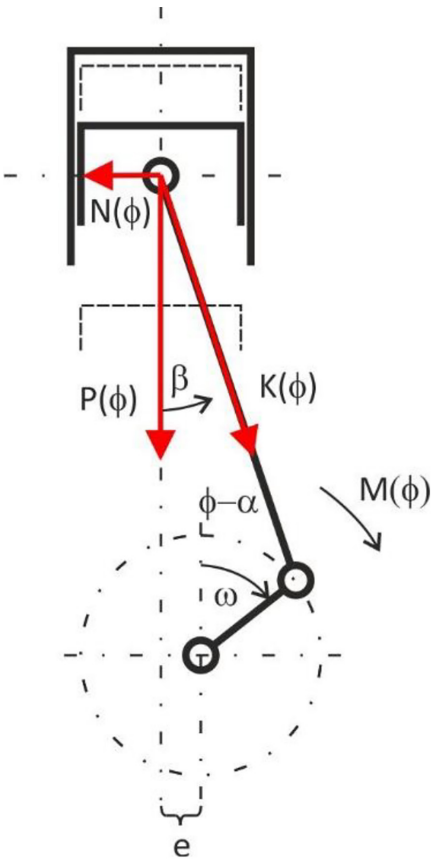


Figure 8. Compression space crank mechanism with crankshaft axis eccentricity (e)

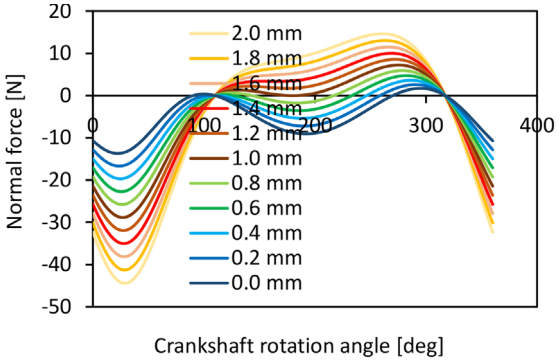


Figure 9. Normal force for positive crankshaft axis eccentricity

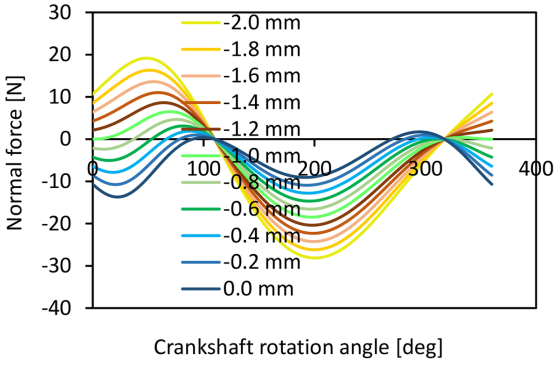


Figure 10. Normal force for negative crankshaft axis eccentricity

the cylinder liner. This solution is commonly used in piston engines, primarily to reduce the number of changes in the sign of the normal force acting on the cylinder liner, which ultimately also reduces the number of piston-to-liner impacts when changing its position from left to right and vice versa. Figure 8 shows a diagram of the modified crankshaft system. Using crankshaft axis eccentricity, the normal force will then be calculated according to the following relationship:

$$N_e(\varphi) = \{[(p(\varphi) - p_o) \cdot S_p] + [P_{in}(\varphi)]\} \cdot \cdot \tan\left\{asin\left[\frac{R \cdot sin(\varphi - \alpha) - e}{L_r}\right]\right\} \quad (18)$$

where: e – crankshaft axis eccentricity.

When crankshaft axis eccentricity is applied, the normal force curve is modified, which also results in changes in the extreme values, amplitude, and number of sign changes within a single

crankshaft revolution. Figures 9 and 10 show the normal force curve for positive and negative crankshaft axis eccentricity values, respectively.

From the perspective of the crankshaft system's impact on the device's structure, the most favourable case occurs when the normal force amplitude is the smallest. A summary of the values is presented in Figure 11.

The obtained results indicate that the lowest normal force amplitude occurs at a negative crankshaft axis eccentricity value of 0.2 mm. This approach allows for a 23% reduction in the analysed case. At the same time, analysing the normal force curves for negative crankshaft axis eccentricity values reveals that an increase in correction below - 0.8 mm causes second-order impacts to cease to dominate and are replaced by first-order impacts, potentially opening the possibility of counteracting the analysed force using a counterweight. Unfortunately, this process comes at the cost of a significant increase in amplitude and, therefore, will not be considered effective for neutralising the normal force. However, partial neutralisation of the normal force, i.e., second-order impacts, using balance shafts has been proposed (Figure 12).

The shafts are equipped with counterweights that rotate at a speed twice that of the crankshaft, and in any position, their vertical components cancel each other out while the horizontal components add up in such a way as to meet the condition:

$$N_{co}(\varphi) = \frac{[max(N_e) - min(N_e)]}{2} \cdot \cdot cos[2 \cdot (\varphi - \varphi_{min})] \quad (19)$$

where: φ_{min} – the angle of rotation of the crankshaft at which the minimum value of the normal force occurs.

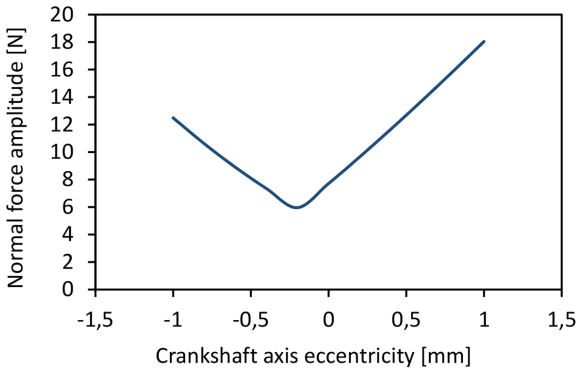


Figure 11. Influence of crankshaft axis eccentricity on normal force

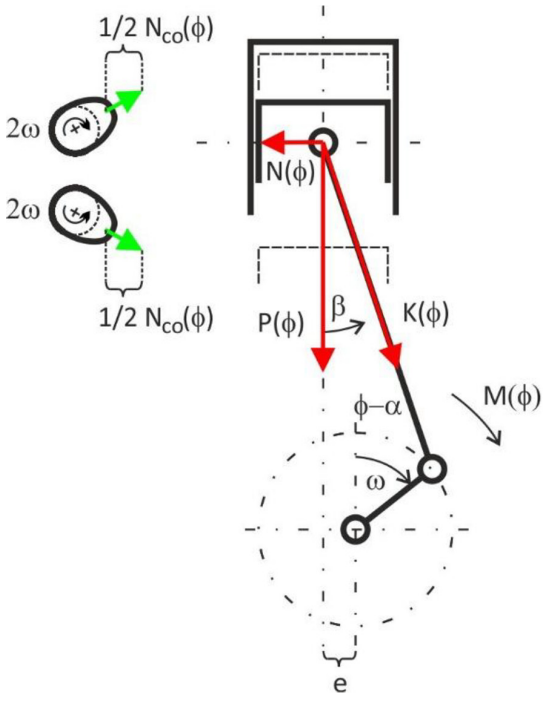


Figure 12. The concept of a crank system with a system balancing the second-order normal force effects (counterweights)

For this balance shaft selection, four cases of crankshaft axis eccentricity were analysed (Figures 13–16). Based on the obtained curves, it can be seen that a significant reduction in the total amplitude occurs for crankshaft axis eccentricity values of 0 and -0.2 mm, while for the values -0.4 mm and -0.6 mm, this reduction is ineffective. Figure 17 summarises all analysed cases of balance shafts neutralising second-order normal force effects. The obtained results indicate that the use of balance shafts produces the best effect for a crankshaft axis eccentricity of -0.2 mm, which, compared to the base case, enables a 63% reduction in the normal force amplitude.

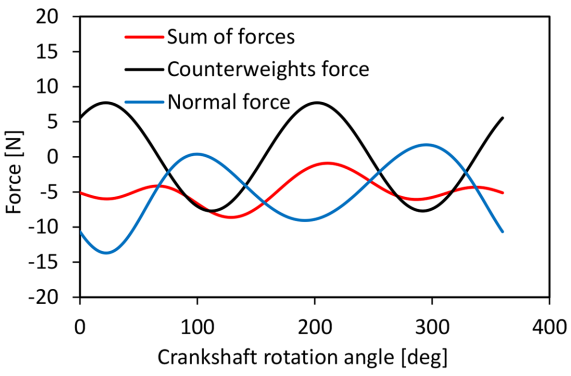


Figure 13. Normal force, second-order counterweights force and the sum of these forces for a crankshaft axis eccentricity of 0.0 mm

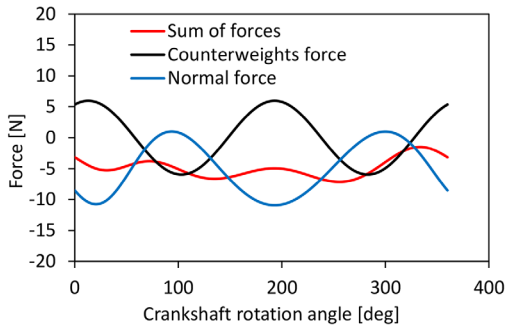


Figure 14. Normal force, second-order counterweights force, and the sum of these forces for a crankshaft axis eccentricity of - 0.2 mm

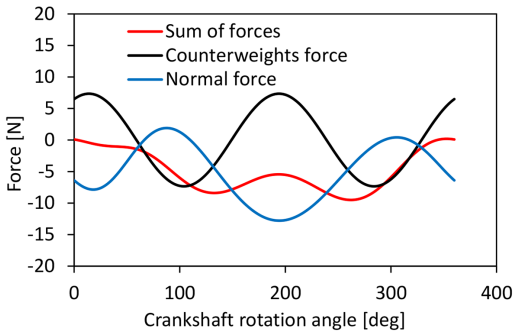


Figure 15. Normal force, second-order counterweights force, and the sum of these forces for a crankshaft axis eccentricity of - 0.4 mm

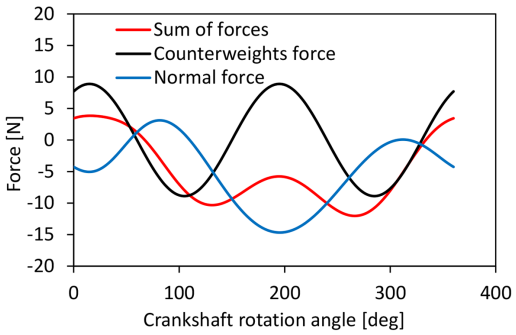


Figure 16. Normal force, second-order counterweights force, and the sum of these forces for a crankshaft axis eccentricity of - 0.6 mm

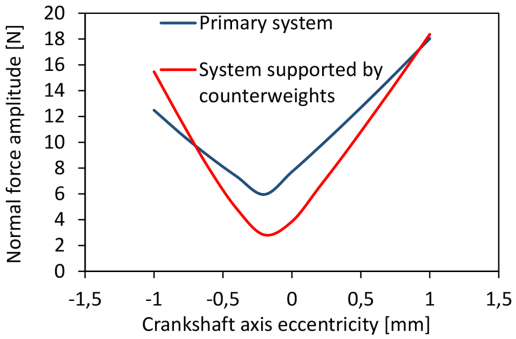


Figure 17. Comparison of the influence of crankshaft axis eccentricity on normal force for the primary system and the system supported by counterweights

CONCLUSIONS

Increasing the bore-to-stroke ratio generally decreases the cooling output of the alpha-type Stirling cryocooler because of the associated increase in dead volume. However, for very small head clearances, below approximately 0.15 mm, this reduction becomes significantly less pronounced. This indicates that a higher bore-to-stroke ratio can be used to reduce the overall dimensions and mass of the cryocooler without substantial performance penalties.

For the analysed configuration with a 0.25 mm head clearance, a bore-to-stroke ratio of approximately 15 provides the most favourable compromise between cooling output and mechanical loading. Although increasing this ratio reduces cooling output, it also decreases the surface pressure on the piston guiding section, improving the durability of the piston-cylinder pair. Introducing a negative crankshaft axis eccentricity of −0.2 mm reduces the amplitude of the normal force acting on the piston guiding section by approximately 23% compared with the conventional mechanism. This demonstrates that crankshaft axis eccentricity is an effective means of reducing piston side loading and, consequently, friction and mechanical wear. The application of balance shafts rotating at twice the crankshaft speed, designed to compensate for second-order forces, further reduces the normal force amplitude. When combined with the optimised crankshaft axis eccentricity, the reduction reaches approximately 63% compared with the conventional mechanism.

The results demonstrate that an appropriate combination of bore-to-stroke ratio, head clearance, crankshaft axis eccentricity, and balance shaft configuration can substantially improve the mechanical performance of an alpha-type Stirling cryocooler while maintaining favourable thermodynamic characteristics. These findings provide practical guidelines for developing more compact, efficient, and durable cryogenic cooling devices. It is worth noting that the practical success of the study's proposed optimisations depends heavily on real-world friction, lubrication, and manufacturing factors. Because miniature Stirling cryocoolers typically operate oil-free to prevent thermal contamination, high normal forces directly accelerate solid lubricant wear and seal degradation on the piston guide section. Furthermore, high normal forces increase friction power losses, which consume

driving power and diminish the overall net efficiency. Thermodynamically, maintaining head clearance below 0.15 mm is crucial for preventing severe cooling output drops, yet machining stack-ups and differential thermal expansion can easily exceed this limit. Mechanically, the optimised -0.2 mm crankshaft eccentricity requires tight positional tolerances, as bearing runout or casing alignment errors shift the effective offset. Finally, the proposed balance shafts require exact angular synchronisation at double rotational speed, where gear backlash or mass tolerances risk introducing parasitic vibrations, rather than cancelling normal forces.

REFERENCES

1. Walker G. Cryocoolers. Part 1: Fundamentals. New York: Plenum Press; 1983.
2. Atrey MD. Cryocooler Technology: The Path to Invisible and Reliable Cryogenics. In: Atrey MD, editor. Cryocoolers: Theory and Applications. Cham: Springer International Publishing; 2020. p. 1–46.
3. Lewis R, et al. Micro cryogenic coolers for IR imaging. In: Infrared Technology and Applications XXXVII. Proc SPIE. 2011;8012:80120K.
4. Shad M, Zhang X. Parametric study of miniature Stirling cryocooler for high temperature infrared detector with design refinement for SWaP configuration. Appl Therm Eng. 2025;273:126495.
5. Sanjay KJ, Senthilkumar S, Kang SW. A study to predict the hydrodynamic and thermal characteristics of hybrid mesh regenerator. Therm Sci Eng Prog. 2024;53:102767.
6. Garg SK, et al. Numerical study of the regenerator for a miniature Stirling cryocooler using the local thermal equilibrium (LTE) and the local thermal nonequilibrium (LTNE) models. Therm Sci Eng Prog. 2019;11:150–161.
7. Shad M, Zhang X. Numerical analysis of cooling performance of a SWaP-refined miniature Stirling cryocooler for higher operating temperature infrared detectors. Cryogenics. 2026;158:104368.
8. Muhammad S, Zhang X. Numerical evaluation of heat transfer characteristics and effectiveness of miniature Stirling cryocooler's regenerator: A multi-part computational study. Cryogenics. 2025;148:104066.
9. Garg SK, et al. Effect of porosity of the regenerator on the performance of a miniature Stirling cryocooler. Therm Sci Eng Prog. 2020;15:100442.
10. Singh M, et al. Development of Miniature Stirling Cryocooler Technology for Infrared Focal Plane Array. Def Sci J. 2013;63(6):571-580.
11. Huang JS, Cheng CH. An efficient theoretical model of rotary-integral Stirling cryocooler validated by experimental testing. Therm Sci Eng Prog. 2023;43:101996.
12. Li R, Grosu L. Parameter effect analysis for a Stirling cryocooler. Int J Refrig. 2017;80:92–105.
13. Sun D, Xu Y, Shen Q. An efficient high cooling capacity Stirling cryocooler and its application for capturing boil-off methane from liquefied natural gas. Int J Refrig. 2024;165:425–433.
14. Li X, et al. A high-efficiency free-piston Stirling cooler with 350 W cooling capacity at 80 K. Energy Procedia. 2019;158:4416–4422.
15. Jang KH, Kim HS, Lee SH. Numerical analysis of free-piston Stirling cooler systems for improving cooling performance. Case Stud Therm Eng. 2022;37:102272.
16. Guo C, Bai Y, Tong L, et al. Quantitative evaluation of a free piston Stirling cooler performance based on a dimensionless analysis method and experimental results. Case Stud Therm Eng. 2026;77:107478.
17. Ding X, et al. Numerical and experimental study on a 20 K high capacity thermally-coupled Stirling-type pulse tube cooler. Energy. 2025;316:134552.
18. Zheng P, et al. Investigation of an efficient high cooling-capacity Stirling-type pulse tube refrigerator with passive rod displacer operating at 173 K. Appl Therm Eng. 2024;248:123142.
19. Luo J, et al. Numerical and experimental study on cooling enhancement of a high-power linear alternator for free-piston Stirling machines. Appl Therm Eng. 2026;287:129462.
20. Jin Q, et al. Experimental and numerical study on radiative cooling of a linear alternator in a free-piston Stirling electric generator. Energy Convers Manag X. 2025;26:101043.
21. Cheng CH, Huang CY. Development of a 100-K pneumatically driven split-type cryogenic Stirling cryocooler based on experimental and numerical study. Cryogenics. 2020;105:102998.
22. Liu B, et al. A high efficiency Stirling/pulse tube hybrid cryocooler operating at 35 K/85 K. Cryogenics. 2019;101:137–140.
23. Sun H, et al. Dynamic and thermodynamic characterization of a resonance tube-coupled free-piston Stirling engine-based combined cooling and power system. Appl Energy. 2022;322:119437.
24. Wei L, et al. Upscaling of thermoacoustic-Stirling duplex cryocoolers based on resonance tube coupling. iScience. 2025;28:113240.
25. Korobko V, et al. Thermoacoustic engines for low-grade heat conversion into mechanical power: A study on oscillation initiation. Appl Therm Eng. 2025;274:126688.

26. Shinozaki K, et al. Cooling performance of Joule Thomson coolers with straight heat exchangers for space science missions. Cryogenics. 2022;128:103575.
27. Kropiwnicki J. Low temperature rotary Stirling engine: conceptual design and theoretical analysis. Appl Therm Eng. 2024;257:124276.
28. Kropiwnicki J. Application of Stirling Engine Type Alpha Powered by the Recovery Energy on Vessels. Pol Marit Res. 2020;27(1):96–106.
29. Rutczyk B, Szczygieł I, Buliński Z. A zero-dimensional, real gas model of an α Stirling engine. Energy Convers Manag. 2019;199:111995.